The 2009 IEEE/RSJ International Conference on
Intelligent Robots and Systems
October 11-15, 2009 St. Louis, USA

Experimental Verification of 3D Bipedal Walking based on Passive Dynamic Autonomous Control

Tadayoshi Aoyama, Kosuke Sekiyama, Yasuhisa Hasegawa, and Toshio Fukuda

Abstract— **This paper addresses a three-dimensional biped dynamic walking control based on Passive Dynamic Autonomous Control (PDAC). In our previous work, the robot dynamics is modeled as a two-dimensional autonomous system of a three-dimensional inverted pendulum by applying the PDAC concept. In addition, the convergence algorithm based on conservative quantities named "PDAC constant" was proposed, so that walking velocity and direction is controllable. In this paper, we apply our control framework to an experimental robot "Multi-locomotion Robot"; then the performance and the efficiency of the proposed control algorithm are verified by experiments.**

I. Introduction

Biped walking control has been studied for many years. The most successful method to realize a three-dimensional dynamic walking is so far the ZMP-based control [1], [2]; however, the ZMP-based control does not use a inherent dynamics of the robot to realize a natural and efficient walking.

So as to realize a natural and efficient walking, some researchers proposed methods to utilize the robot dynamics directly, assuming a point-contact between the robot foot and the ground. Kajita *et al.* proposed a control method which employed the conserved quantity introduced by the assumption of the horizontal COG (Center Of Gravity) trajectory [3]. Ono *et al.* proposed the self-exited walking of the underactuated robot [4]. Chevallereau presented the control of the robot dynamics on an optical trajectory by introducing the virtual time [5]. Grizzle and Westervelt *et al.* built the controller by the use of virtual holonomic constraint of joints named *Virtual Constraint* which realizes the stable dynamic walking by means of the biped robot with a torso [6]–[8]. Some of these point-contact methods realized smooth dynamic walking with two-dimensional experimental robots.

Also, it is reported that three bipedal robots, where minimum actuations based on passive dynamic walker [9] are applied, realized three dimensional natural and efficient walking on the level ground [10]. Although their work paid attention to energy efficiency, the analytical control law was not emphasized. On the other hand, there are some interesting researches proposing analytical three-dimensional biped walking control law based on point-contact method for a five-link bipedal robot [11], [12]; however, experimental validations are not found in these works.

Fukuda *et al.* realized three-dimensional dynamic walking with the experimental robot based on the assumption that the sagittal and lateral motion can be separated [13]. However, this control method has a problem in dividing three-dimensional dynamics when the dynamics of each plane are closely coupled. In order to solve this problem, Doi *et al.* proposed Passive Dynamic Autonomous Control (PDAC) [14] and applied it to three-dimensional natural biped walking with an experimental robot [15].

We extended the PDAC further and proposed a stabilizing method of three-dimensional biped walking previously [16], which was only verified by numerical simulations. It is important to verify the performance of the proposed control algorithm by using an actual robot. In this paper, we apply the convergent controller and the walking direction controller in the work [16] to the experimental robot "Multi-locomotion Robot [17]"; then the performance and the efficiency of the proposed control algorithm are verified by experiments.

II. Passive Dynamic Autonomous Control (PDAC)

The PDAC was proposed previously by Doi based on two concepts, i.e. point-contact and virtual constraint [14]. Point-contact means that a robot contacts the ground at a point, that is, the first joint is passive. Virtual constraint was defined by Grizzle and Westervelt *et al.* [6], [8] as a set of holonomic constraints on the robot's actuated DoF parameterized by the robot's unactuated DoF. Assuming that PDAC is applied to the serial n-link rigid robot as shown in Fig. 1, these two premises are expressed as follows:

$$\tau_1 = 0 \tag{1}$$

$$\begin{aligned}\boldsymbol{\Theta} &= [\theta_1, \theta_2, \cdots, \theta_n]^T = [f_1(\theta), f_2(\theta), \cdots, f_n(\theta)]^T \\ &:= \boldsymbol{f}(\theta),\end{aligned} \tag{2}$$

where θ is the angle around the contact point w.r.t the absolute coordinate system, that is, $\theta_1 = f_1(\theta) = \theta$.

The whole robot dynamics is expressed as the following one-dimensional autonomous system (that is, the phase around contact point),

$$\dot{\theta} = \frac{1}{M(\theta)}\sqrt{2\int M(\theta)G(\theta)\, d\theta} \tag{3}$$

$$:= \frac{1}{M(\theta)}\sqrt{2\big(D(\theta) + C\big)} \tag{4}$$

$$:= F(\theta). \tag{5}$$

T. Aoyama and K. Sekiyama and T. Fukuda are with the Department of Micro-Nano Systems Engineering, Nagoya University, Furo-cho-1, Chikusa-ku, Nagoya, 464-8603, JAPAN aoyama@robo.mein.nagoya-u.ac.jp, sekiyama, fukuda@mein.nagoya-u.ac.jp

Y. Hasegawa is with the Department Intelligent Interaction Technologies, University of Tsukuba, 1-1-1 Tenodai, Tsukuba, 305-8573, JAPAN hase@esys.tsukuba.ac.jp

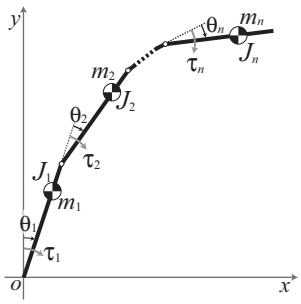

Fig. 1. Mechanical model of the serial n-link rigid robot. θ_i and τ_i are the angle and the torque of ith joint respectively. m_i and J_i are the mass and the moment of inertia of ith link respectively.

The detailed calculation process is given in [14]. In this paper, we term Eq. (4) and (5) as the Converged dynamics.

Since the Converged dynamics is autonomous, in addition, independent of time, it is considered as a conservative system. The integral constant in right hand side of Eq. (4) C, is a conserved quantity, which is termed as the PDAC constant. Its value is determined according to the initial condition (as for biped walking, the state immediately after foot-contact), and kept constant during a cycle of motion. Thus, it is possible to stabilize the motion by keeping the PDAC constant at a certain value.

III. Derivation of Converged Dynamics

As for humanoid-type robots, the trunk has much larger mass compared to the limbs. Thus, in this paper, a robot is modeled as a three-dimensional inverted pendulum shown in Fig. 2(a). We apply an assumption of the point-contact to this pendulum in accordance with the PDAC, hence it is possible to choose the axes of pendulum angle around the contact point to express its motion. In this paper, we utilize the polar coordinate system. The state variables and parameters are shown in Fig. 3(b). θ and ϕ are the variables of the pendulum angle around the contact point. l is the variable of the pendulum length.

In this paper, the trunk inclination is kept in the gravitational direction and the upper body does not rotate around yaw-axis. In addition, we assume that the robot is symmetrical. By applying PDAC, dynamic equations of three-dimensional inverted pendulum are expressed as follows:

$$\frac{d}{dt}\left(ml^2\sin^2\theta\dot{\phi}\right) = 0 \tag{6}$$

$$\frac{d}{dt}\left(ml^2\dot{\theta}\right) = ml^2\dot{\phi}^2\sin\theta\cos\theta + mgl\sin\theta. \tag{7}$$

The detailed calculation process of Eq. (6), (7) is given in [15]. By multiplying both sides of Eq. (6) by $ml^2\sin^2\theta\dot{\phi}$, and integrating with respect to time, the following constraint equation is obtained,

$$\dot{\phi} = \frac{\sqrt{2C_1}}{ml^2\sin^2\theta} \tag{8}$$

$$:= F_1(\theta), \tag{9}$$

where C_1 is the integral constant which is determined by initial state immediately after foot-contact. Substituting Eq. (8) into Eq. (7) results in

$$\dot{\theta} = \frac{1}{ml^2}\sqrt{2\int\left(\frac{2C_1\cos\theta}{\sin^3\theta} + m^2gl^3\sin\theta d\theta\right)} \tag{10}$$

$$:= \frac{1}{M(\theta)}\sqrt{2\big(D(\theta)+C_2\big)} \tag{11}$$

$$:= F_2(\theta). \tag{12}$$

Next, in accordance with PDAC, the pendulum length is described as the function of θ,

$$l := \lambda(\theta). \tag{13}$$

In this paper, for simplicity, λ is defined as the following function of θ,

$$\lambda(\theta) =: \sqrt[3]{p_1\theta^3 + p_2\theta^2 + p_3\theta^+ p_4} \tag{14}$$

$$=: \sqrt[3]{f(\theta)}. \tag{15}$$

By substituting this equation into Eq. (11), the converged dynamics is derived,

$$M(\theta) = mf(\theta)^{2/3} \tag{16}$$

$$D(\theta) = -\frac{C_1}{\sin^2\theta} - m^2g\Big(\big(f(\theta)-f''(\theta)\big)\cos\theta - \big(f'(\theta)-f'''(\theta)\big)\sin\theta\Big). \tag{17}$$

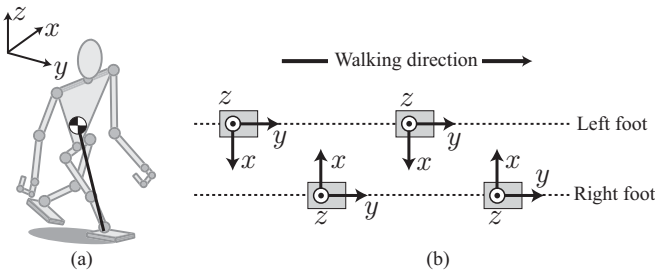

Fig. 2. (a) 3D inverted pendulum model. (b) Definition of coordinate system. Note that this figure shows just a coordinate system definition and doesn't mean that foot placement is in alignment.

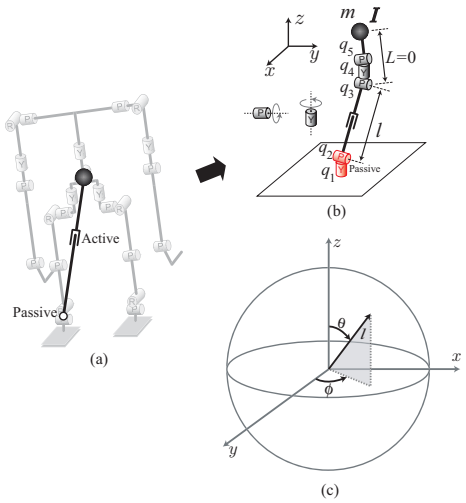

Fig. 3. (a) Passive joints (point-contact) and active pendulum length actuation. (b) Polar coordinate system around contact point.

IV. Design of Controller

A. Design of walking cycle

In this subsection, the actual motion of the robot is designed. Figure 4 shows the schematics of the pendulum

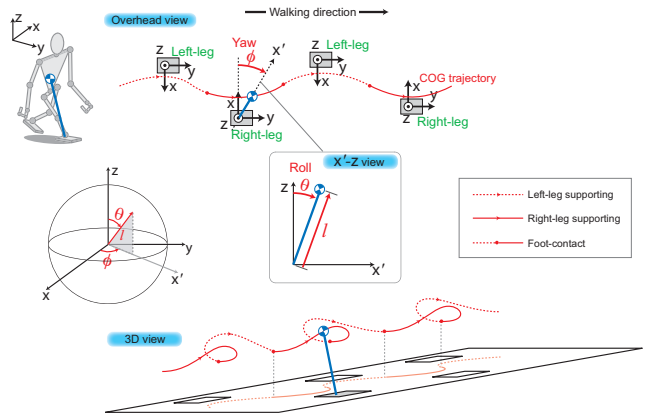

Fig. 4. Motion of a 3D inverted pendulum.

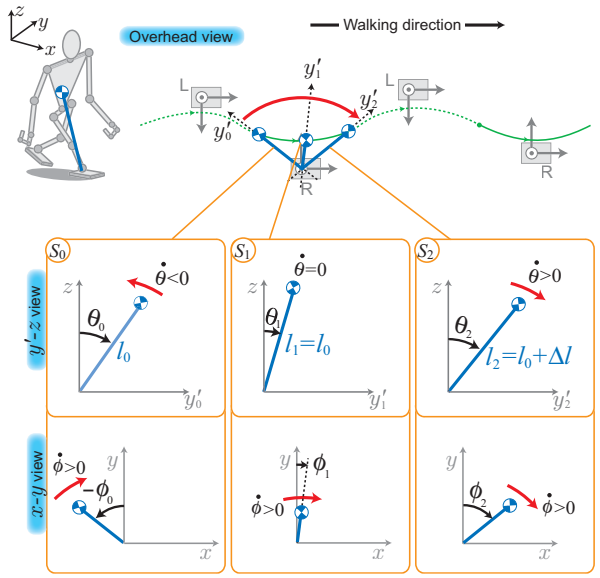

Fig. 5. Parameters and variables of dynamic walking based on 3D inverted pendulum model.

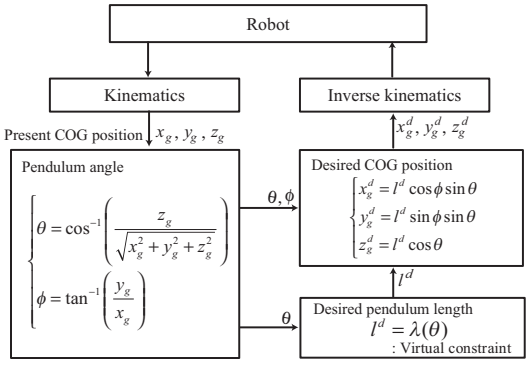

Fig. 6. COG controller based on virtual constraint

motion and the COG trajectory of the biped walking. The continuous line shows a trajectory of the COG in the right-leg support phase and the dotted line shows in the left-leg support phase. The dot on the edge of both the continuous line and the dotted one means a foot-contact. Figure 5 shows the parameters and variables. S_0 and S_2 denote moments right before and after a foot-contact, and S_1 is the moment at $\dot{\theta} = 0$. θ_i, ϕ_i, and l_i denote the roll angle, yaw angle, and pendulum length at S_i $(i = 0, 1, 2)$ respectively. During the cycle of walking motion, ϕ will monotonically increase. Meanwhile, θ will decrease at first, and then increases, after posing for a moment at θ_1. Thus, decompose the walking cycle from a foot-contact to the next foot-contact into two phases—Phase (A): from S_0 to S_1 $(\dot{\theta} < 0)$, Phase (B): from S_1 to S_2 $(\dot{\theta} > 0)$. In the phase (A), the pendulum length will not change, thus

$$p_1 = p_2 = p_3 = 0, \tag{18}$$
$$p_d = l_0^3. \tag{19}$$

In the phase (B), the coefficients p_1-p_4 are decided so that the following four conditions are satisfied,

$$f(\theta_1) = l_1^3, \tag{20}$$
$$f(\theta_2) = l_2^3, \tag{21}$$
$$f'(\theta_2) = 0, \text{ and} \tag{22}$$
$$-f''(\theta_1)\cos\theta_1 + \big(-f'(\theta_1) + f'''(\theta_1)\big)\sin\theta_1 = 0. \tag{23}$$

Eqs. (20) and (21) indicate the continuity condition of the pendulum length, and Eq. (22) is the condition that the velocity of pendulum along l is 0 in the foot-contact. The objective of Eq. (23) is to adjust PDAC constants of the phase (A) and (B). In the phase (A), conditions of $f'(\theta) = 0$, $f''(\theta) = 0$, and $f'''(\theta) = 0$ are satisfied because the pendulum length is the constant value, i.e. $f(\theta) = l_0^3$. Thus, if Eq. (23) holds when $\theta = \theta_1$, Eq. (17) that is converged dynamics, is continual during a walking cycle and PDAC constants remain constant during a step.

From Eqs. (20)-(23), the coefficients p_1-p_4 are derived as follows:

$$p_1 = -\frac{l_2^3 - l_0^3}{(\theta_2 - \theta_1)^2}\frac{u_3}{u_1 u_3 - u_2}, \tag{24}$$
$$p_2 = -\frac{l_2^3 - l_0^3}{(\theta_2 - \theta_1)^2}\frac{u_2}{u_1 u_3 - u_2}, \tag{25}$$
$$p_3 = -3p_1\theta_2^2 - 2p_2\theta_2, \text{ and} \tag{26}$$
$$p_4 = l_2^3 - p_1\theta_2^3 - p_2\theta_2^2 - p_3\theta_2, \tag{27}$$

where

$$u_1 = 2\theta_2 + \theta_1, \tag{28}$$
$$u_2 = -6\theta_1\cos\theta_1 - 3\theta_1^2\sin\theta_1 + 6\sin\theta_1 + 3\theta_2^2\sin\theta_1, \text{ and} \tag{29}$$
$$u_3 = -2\cos\theta_1 - 2\theta_1\sin\theta_1 + 2\theta_2\sin\theta_1. \tag{30}$$

B. COG controller based on virtual constraint

Figure 6 shows the block diagram of the robot joint control based on virtual holonomic constraint. The current COG

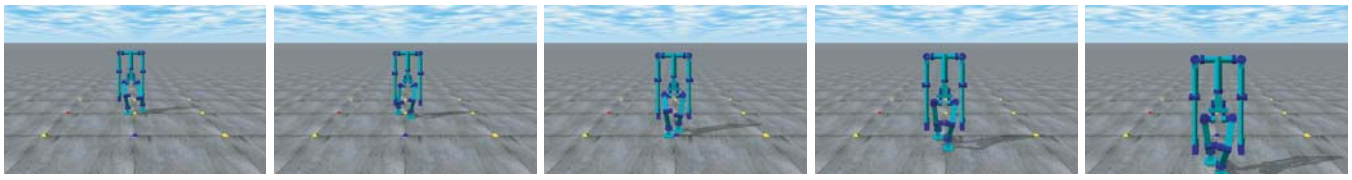

(a)C_1=0.46, C_2=566.58 (b)C_1=0.43, C_2=567.38 (c)C_1=0.42, C_2=570.30 (d)C_1=0.37, C_2=571.34 (e)C_1=0.24, C_2=571.29

Fig. 7. Snapshots of the Simulation

position, (x_g, y_g, z_g) is derived by solving the forward kinematics. From this result, pendulum angles can be determined as below,

$$\theta = \cos^{-1}\left(\frac{z_g}{\sqrt{x_g^2 + y_g^2 + z_g^2}}\right), \tag{31}$$

$$\phi = \tan^{-1}\left(\frac{y_g}{x_g}\right). \tag{32}$$

By use of θ, the desired pendulum length is calculated,

$$l^d = \lambda(\theta). \tag{33}$$

Consequently, the desired COG position is derived as follows:

$$x_g^d = l^d \cos\phi \sin\theta, \tag{34}$$

$$y_g^d = l^d \sin\phi \sin\theta, \text{ and} \tag{35}$$

$$z_g^d = l^d \cos\theta. \tag{36}$$

The desired joint angles are decided by solving the inverse kinematics with reference to the desired COG position.

C. Foot-contact model

In this paper, it is assumed that perfectly inelastic collision between a ground and a foot occurres for a moment similarly to previous works [6], [8], [18], [19]. Thus the angular momentum around a new contact point is conserved. Assuming that ϕ_0 is the angle of ϕ right after a foot-contact, a vector of the pendulum after impact, $\boldsymbol{L}$ is

$$\boldsymbol{L} = [l_0 \sin\phi_0 \sin\theta_0, l_0 \cos\phi_0 \sin\theta_0, l_0 \cos\theta_0]^T, \tag{37}$$

where ϕ_0 and θ_0 are angles in the coordinate system of the next step.

The velocity vector right before a foot-contact, $\boldsymbol{V_1}$, is calculated as follows:

$$\boldsymbol{V_1} = [v_x, v_y, v_z]^T, \tag{38}$$

where

$$\begin{aligned} v_x =& l_2(\dot{\phi}_2 \cos\phi_2 \sin\theta_2 + \dot{\theta}_2 \sin\phi_2 \cos\theta_2) \\ &+ \dot{l}_2(\sin\phi_2 \sin\theta_2), \\ v_y =& l_2(-\dot{\phi}_2 \sin\phi_2 \sin\theta_2 + \dot{\theta}_2 \cos\phi_2 \cos\theta_2) \\ &+ \dot{l}_2(\cos\phi_2 \sin\theta_2), \\ v_z =& -l_2\dot{\theta}_2 \sin\theta_2 + \dot{l}_2(\cos\theta_2), \text{ and} \end{aligned}$$

ϕ_2 is the angle of ϕ before the foot-contact.

The velocity vector after the foot-contact, $\boldsymbol{V_0}$, is derived by the following equation,

$$\boldsymbol{V_0} = \frac{\boldsymbol{V_1} \cdot (\boldsymbol{L} \times (\boldsymbol{V_1} \times \boldsymbol{L}))}{|\boldsymbol{L} \times (\boldsymbol{V_1} \times \boldsymbol{L})|} (\boldsymbol{L} \times (\boldsymbol{V_1} \times \boldsymbol{L})) \tag{39}$$

$$= \frac{\boldsymbol{L} \times (\boldsymbol{V_1} \times \boldsymbol{L})}{l^2} \tag{40}$$

$$:= [v'_x, v'_y, v'_z]^T. \tag{41}$$

Note that $\boldsymbol{V_1}$ is $[-v_x, v_y, v_z]$ since left- and right-handed systems are switched at the foot-contact.

From Eq. (41), $\dot{\theta}_0$ and $\dot{\phi}_0$ are

$$\dot{\theta}_0 = -\frac{v'_z}{l_0 \sin\theta_0}, \tag{42}$$

$$\dot{\phi}_0 = -\frac{\sin\phi_0 \cos\theta_0}{\cos\phi_0 \sin\theta_0}\dot{\theta}_0 - \frac{v'_x}{l_0 \cos\phi_0 \sin\theta_0}. \tag{43}$$

V. Experiment

A. Simulation

In this paper, we apply the convergent controller and the walking direction controller in our previous work [16] for stabilization of a bipedal walking. By these controllers, two PDAC constants C_1 and C_2 converge to C_1^* and C_2^* that are desired values of PDAC constant; then the robot dynamics converges to a unique trajectory in the four-dimensional space composed of θ, ϕ, $\dot{\theta}$, and $\dot{\phi}$. In the control framework, a step-length, a walking period, and a walking velocity are determined by the desired PDAC constants C_1^*, C_2^* and COG height at a foot-contact h. Unfortunately, we have not found yet the systematic method to acquire the optimal combination of C_1^*, C_2^*, and h according to the desired step-length, walking period, and walking velocity. Thus, in this paper, applicable C_1^*, C_2^* and h for the actual robot are determined empirically by numerical simulations. As the results of the simulations considered the physical parameters of the Gorilla Robot Ⅲ (introduced in the next subsection), applicable C_1^*, C_2^* ,and h are found as follows; C_1^*=[(Kgm^2/s)^2], C_2^*=[(Kgm^2/s)^2], and h=0.48[m]. On the condition that these parameters are applied, also initial conditions of velocity are set as $\dot{\theta}$=0.1[rad/sec], $\dot{\phi}$=0.0[rad/sec], the step length, the walking period and the walking velocity converge to 0.18[m], 0.65[sec], and 0.28[m/s] respectively. Figure 7 shows snapshots of this simulation.

B. Experimental setup

Figure 8 depicts the overview of our robot "Gorilla Robot Ⅲ(Multi-Locomotion Robot) [17]" and its link structure. The

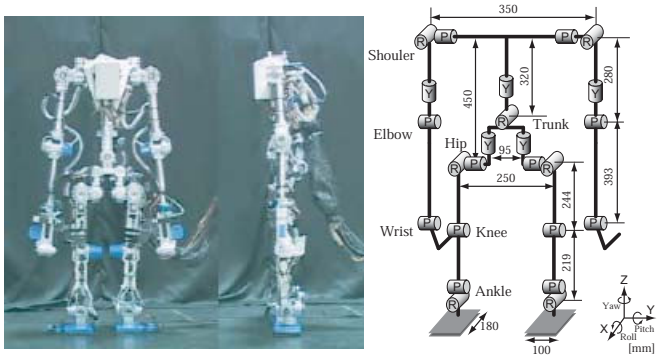

Fig. 8. Gorilla Robot Ⅲ(Multi-Locomotion Robot) [17]. This robot is multi-locomotive; it can perfome biped locomotion, quadruped locomotion and brachiation.

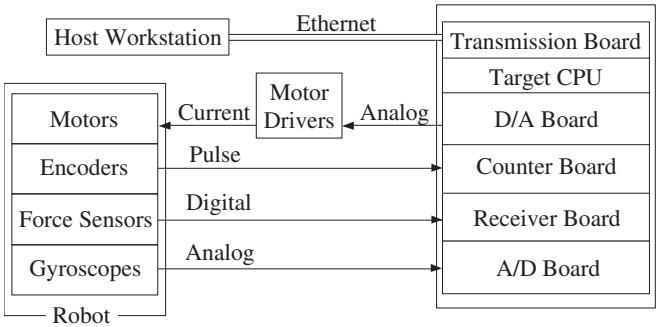

Fig. 9. Control System of Gorilla Robot Ⅲ

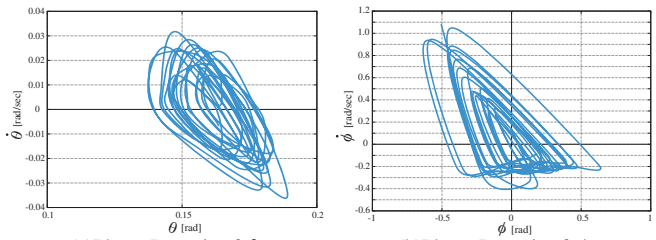

(a)Phase Portrait of θ (b)Phase Portrait of ϕ

Fig. 10. Phase Portrait of the inverted pendulum.

robot is about 1.0[m] tall, weighs about 24.0[kg], and consists of 25 links and 24 motors including two grippers. The real-time operating system VxWorks (Wind River Systems) runs on a Pentium Ⅲ PC for processing sensory data and generating its behaviors. Each joint is driven by AC servo motor through the harmonic drive gear, partially through a timing belt. Maximum output power of the motor is 30[W]. The power supply and the computer are installed outside of the robot for weight saving. The control system of the Gorilla Robot Ⅲ is shown as Fig. 9.

C. Experimental result

We validated the proposed algorithm with the Gorilla Robot Ⅲ. The experiment was conducted on the level ground with maximum $\pm$1.0[cm] irregularity. As a result of the experiment, three-dimensional dynamic walking in 0.14[m] step-length and 0.26[m/s] walking velocity was realized. Although the ground has maximum $\pm$1.0[cm] irregularity in the experimental environment and the information of the ground shape was not given to the robot, the robot achieved

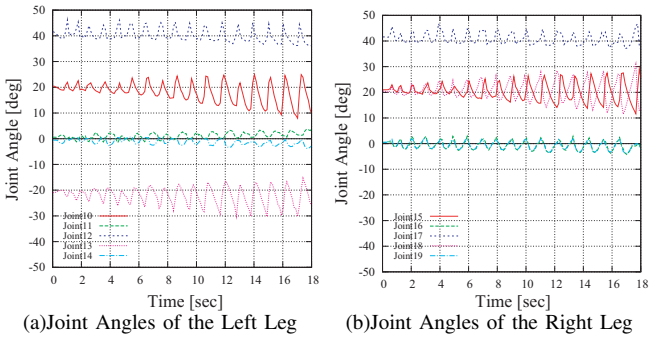

(a)Joint Angles of the Left Leg (b)Joint Angles of the Right Leg

Fig. 11. Joint angle of the bipedal walking experiment.

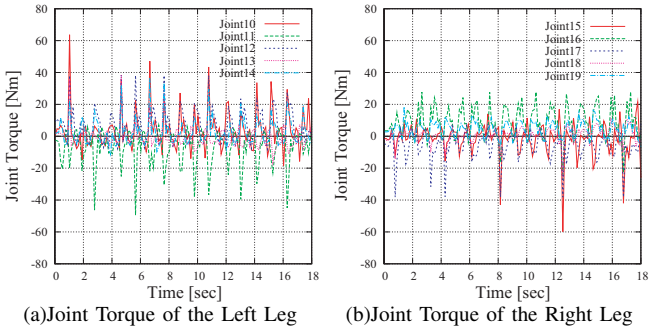

(a)Joint Torque of the Left Leg (b)Joint Torque of the Right Leg

Fig. 12. Torque output of the bipedal walking experiment.

the stable walking without information of the ground. Figure 10 shows the phase portrait of the inverted pendulum. From this figure, it is confirmed that the inverted pendulum motion doesn't diverge but make a periodic motion. Figures 11 and 12 show the joint angles and joint torques of the experiment respectively. Also, Fig. 13 shows snapshots of the experiment.

D. Energy efficiency

In this paper, in order to compare an energy efficiency between robots of different sizes, the dimensionless specific cost of transport, C_t=(energy used)/(weight$\times$distance traveled) which was proposed in [10], and the specific energetic cost of transport, C_{et}, and the specific mechanical cost of transport, C_{mt} were defined. Whereas C_{et} uses the total energy consumed by the system, C_{mt} considers the positive mechanical work of the actuators. Since a total energy cannot be evaluated in our system, this paper uses C_{mt} as the energetic cost of transport. The mechanical work of the actuators in one cycle of the walking E is calculated as follows:

$$E = \int_0^T \sum_{i=1}^{N} \delta\left(\tau_i \dot{\theta}_i\right) dt, \tag{44}$$

$$\delta(x) = \begin{cases} x, & if\ x > 0 \\ 0, & if\ x \leq 0 \end{cases}, \tag{45}$$

where T is the cycle time of a walk, N is the number of actuators, τ_i and $\dot{\theta}_i$ are the joint torque and the angular velocity of i-th joint number. Then, the mechanical cost of transport C_{mt} in one cycle of a walk is calculated as follows:

$$C_{mt} = \frac{E}{S \times Mg}, \tag{46}$$

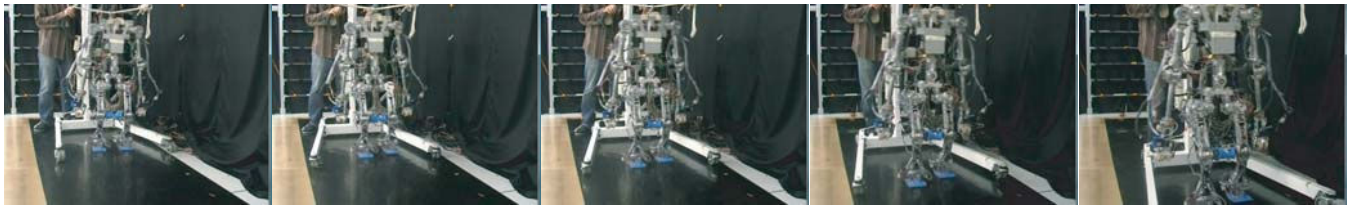

(a) (b) (c) (d) (e)

Fig. 13. Snapshots of the Bipedal Walking Experiment. Each figure shows the snapshots at (a)1st (b)7th (c)13th (d)19th (e)25th step.

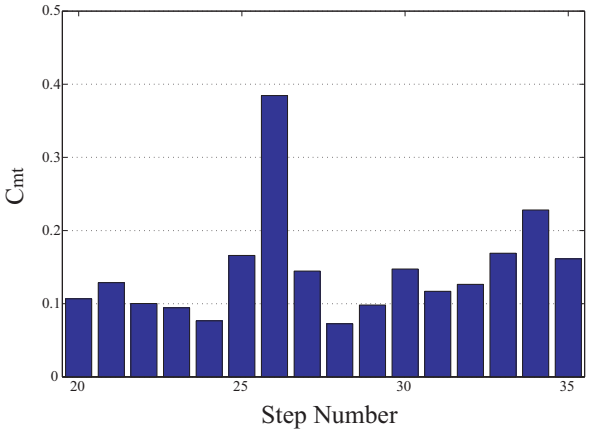

Fig. 14. C_{mt} estimated from experimental data.

where S is the step length of the robot, M is the mass of the robot, g is the gravitational acceleration. After 20 steps, the motion of the robot converges to the stable one. The experimental C_{mt} of each step are shown in Fig. 14, and the average of C_{mt} is 0.15. The C_{mt} of Honda humanoid ASIMO [20] which realized a stable three-dimensional dynamic walking applied ZMP-based control is estimated 1.6 in [10], thus our walking algorithm is efficient more than ten times compare to the ZMP-based control.

VI. Conclusion

This paper realized a PDAC-based three-dimensional biped dynamic walking on the level ground. The robot dynamics is modeled as a two-dimensional autonomous system of a three-dimensional inverted pendulum by applying the PDAC; then two conservative quantities named PDAC constant were derived. We applied the convergent controller and the walking direction controller based on PDAC constants to the Multi-locomotion robot. The applicable desired PDAC constants C_1^* and C_2^* for the robot were determined by numerical simulations. Finally, experimental results validated the performance and the energy efficiency of the PDAC-based bipedal walking algorithm.

References

[1] S. Kajita, M. Morisawa, K. Harada, K. Kaneko, F. Kanehiro, K. Fujiwara, and H. Hirukawa, "Biped Walking Pattern Generator allowing Auxiliary ZMP Control," in *Proceedings of the IEEE/RSJ International Conference on Intelligent Robots and Systems*, 2006, pp. 2993–2999.

[2] T. Takubo, Y. Imada, K. Ohara, Y. Mae, and T. Arai, "Rough Terrain Walking for Bipedal Robot by Using ZMP Criteria Map," in *Proceedings of the IEEE International Conference on Robotics and Automation*, 2009, pp. 788–793.

[3] S. Kajita, T. Yamaura, and A. Kobayashi, "Dynamic walking control of a biped robot along a potential energy conserving orbit," *IEEE Transactions on Robotics and Automation*, vol. 8, no. 4, pp. 431–438, 1992.

[4] K. Ono, T. Furuichi, and R. Takahashi, "Self-Excited Walking of a Biped Mechanism With Feet," *The International Journal of Robotics Research*, vol. 23, no. 1, pp. 55–68, 2004.

[5] C. Chevallereau, "Time-Scaling Control for an Underactuated Biped Robot," *IEEE Transactions on Robotics and Automation*, vol. 19, no. 2, pp. 362–368, 2003.

[6] J. W. Grizzle, G. Abba, and F. Plestan, "Asymptotically Stable Walking for Biped Robots: Analysis via Systems with Impulse Effects," *IEEE Transactions on Automatic Control*, vol. 46, no. 1, pp. 51–64, 2001.

[7] E. R. Westervelt, J. W. Grizzle, and D. E. Koditschek, "Hybrid Zero Dynamics of Planar Biped Walkers," *IEEE Transactions on Automatic Control*, vol. 48, no. 1, pp. 42–56, 2003.

[8] E. R. Westervelt, G. Buche, and J. Grizzle, "Experimental Validation of a Framework for the Design of Controllers that Induce Stable Walking in Planar Bipeds," *The International Journal of Robotics Research*, vol. 23, no. 6, pp. 559–582, 2004.

[9] T. McGeer, "Passive Dynamic Walking," *The International Journal of Robotics Research*, vol. 9, no. 2, pp. 62–82, 1990.

[10] S. Collins, A. Ruina, R. Tedrake, and M. Wisse, "Efficient Bipedal Robots Based on Passive-Dynamic Walkers," *Science*, vol. 307, pp. 1082–1085, 2005.

[11] G. Song and M. Zefran, "Underactuated Dynamic Three-Dimensional Bipedal Walking," in *Proceedings of the IEEE International Conference on Robotics and Automation*, 2006, pp. 854–859.

[12] C. Chevallereau, J. W. Grizzle, and C.-L. Shih, "Asymptotically Stable Walking of a Five-Link Underactuated 3-D Bipedal Robot," *IEEE Transactions on Robotics*, vol. 25, no. 1, pp. 37–50, 2009.

[13] T. Fukuda, M. Doi, Y. Hasegawa, and H. Kajima, *Fast Motions in Biomechanics And Robotics: Optimization And Feedback Control*. Springer-Verlag, 2006, chapter Multi-Locomotion Control of Biped Locomotion and Brachiation Robot, pp. 121-145.

[14] M. Doi, Y. Hasegawa and T. Fukuda, "Passive Dynamic Autonomous Control of Bipedal Walking," in *Proceedings of the IEEE/RAS International Conference on Humanoid Robots*, 2004, pp. 811– 829.

[15] M. Doi, Y. Hasegawa, and T. Fukuda, "3D Dynamic Walking based on the inverted pendulum model with two degree of underactuation," in *Proceedings of the IEEE/RSJ International Conference on Intelligent Robots and Systems*, 2005, pp. 2788–2793.

[16] T. Aoyama, K. Sekiyama, Y. Hasegawa, and T. Fukuda, "PDAC-based Underactuated 3D Bipedal Walking -Stabilization of PDAC Constants and Walking Direction Control-," in *Proceedings of the IEEE International Conference on Robotics and Automation*, 2009, pp. 1564–1570.

[17] H. Kajima, M. Doi, Y. Hasegawa, and T. Fukuda, "Study on Brachiation Controller for the Multi-locomotion Robot -Redesigning Behavior Controllers-," in *Proceeding of the IEEE/RSJ International Conference on Intelligent Robots and Systems*, 2003, pp. 1388–1393.

[18] A. D. Kuo, "Stabilization of Lateral Motion in Passive Dynamic Walking," *The International Journal of Robotics Research*, vol. 18, no. 9, pp. 917–930, 1999.

[19] A. Goswami, B. Espiau, and A. Keramane, "Limit cycles in a passive compass gait biped and passivity-mimicking control laws," *Autonomous Robots*, vol. 4, pp. 274–286, 1997.

[20] Y. Sakagami, R. Watanabe, C. Aoyama, S. Matsunaga, N. Higaki, and K. Fujimura, "The intelligent ASIMO: System overview and integration," in *Proceedings of the IEEE/RSJ International Conference on Intelligent Robots and Systems*, 2002, pp. 2478–2483.